Relative humidity over ice as a key variable for Northern hemisphere extratropical tropopause inversion layers

Daniel Köhler[1,*], Philipp Reutter[1], and Peter Spichtinger[1]

[1]Institute for Atmospheric Physics, Johannes Gutenberg University Mainz, Mainz, Germany
[*]now at University of Helsinki, Helsinki, Finland

Correspondence: Philipp Reutter (preutter@uni-mainz.de)

Abstract.

The tropopause inversion layer (TIL) is a prominent feature of the (extratropical) tropopause region, as it constitutes a transport barrier. Adiabatic and diabatic processes might contribute to the formation and sharpening of the inversion. For both types of processes, the relative humidity over ice is an ideal quantity for attribution; from theory and former model case studies we would expect enhanced relative humidity values in connection with a sharp TIL.

We use high resolution radiosonde data in comparison with ERA5 reanalysis data to show that there is a very good qualitative and quantitative agreement in terms of TIL features; thus, the coarser ERA5 data can be used for further investigations. In a second step, we investigate the the connection between TIL features and relative humidity measures in both, radiosonde and ERA5 data; here, a clear relationship becomes evident. Moister profiles, on average, exhibit significantly higher maximum values of the Brunt-Väisälä frequency N^2, indicating a more stable stratification of the tropopause in these cases. This result holds true in both radiosonde measurements and ERA5 data. Considering the thickness of the TIL layer, an inverse pattern emerges. In this case, moister and more stable TILs exhibit a lower thickness.

Because of the good agreement between radiosonde and ERA5 data, we extent the investigation using solely ERA5 data for seasonal and regional investigations. These analyses reveal consistent relationships in various extratropical regions of the Northern Hemisphere under different meteorological conditions. Differences in the strength of the dependence of TIL properties on relative humidity over ice are evident.

1 Introduction

The Earth's atmosphere, a dynamic and complex multiscale system, plays a pivotal role in regulating our planet's climate and weather patterns. Within this intricate atmospheric structure lies the troposphere, the layer closest to the Earth's surface and the site of most of our planet's weather phenomena. At its upper boundary to the adjacent stratosphere, the static stability is highly increasing until reaching stratospheric values. This transition layer of increasing stability is often called tropopause region, with more or less strict definitions (see, e.g., Gettelman et al., 2011). About 20 years ago, Birner et al. (2002) were able to demonstrate with high-resolution radiosonde data that sometimes the troposphere encounters a strong temperature inversion known as the tropopause inversion layer (TIL). This feature is most prominent, if the vertical coordinate system is transformed

into a system utilizing the thermal tropopause as the reference point for the vertical coordinate instead of sea level. Sometimes, averaging methods are additionally used to demonstrate the main features on a larger vertical scale.

Situated at the interface between the troposphere and the stratosphere, the TIL represents a unique and enigmatic region characterized by an abrupt increase in temperature with altitude — a significant departure from the typical decrease in temperature observed throughout the lower atmosphere. Thus, a sharp TIL constitutes a strong transport barrier for trace gases, cloud particles, and other key variables like vertical motion. Beyond this the importance of the TIL also lies within the diagnostics of upper troposphere and lower stratosphere (UTLS) structures.

Since its discovery, a couple of hypotheses were developed to explain the origin and formation of the TIL. Wirth and Szabo (2007) showed in model analyses that baroclinic waves lead to a net sharpening of the tropopause, which leads to a stronger TIL. Gettelman and Wang (2015) and Randel et al. (2007) provided further evidence to support the impact of baroclinic waves on the TIL. Additionally, Randel et al. (2007) suggested a radiative forcing mechanism, where the interaction of ozone and water vapour with radiation are contributing to the TIL formation and persistence.

In a recent model study, Kunkel et al. (2016) were able to show that the formation of the TIL is probably driven by a combination of different adiabatic and diabatic processes. In a first step, evolving baroclinic instabilities lead to a compression of isentropes, which in turn results into sharper gradients of the stability. Relevant processes in this respect are horizontal convergence in anticyclonic regions, strong upward motions, e.g. triggered by convective instabilities, and gravity waves triggered by the large scale flow, respectively. Since these changes are mostly adiabatic and thus reversible in general, in a second step diabatic processes as turbulence/mixing, cloud formation and resulting latent heat release and radiative heating/cooling by trace gases (as water vapor) modify the TIL irreversible. As showed by Kunkel et al. (2016), the diagnostics of these processes is quite difficult and from measurements it might be quite impossible to disentangle the contributions of the different processes.

However, by careful inspection of the scenario, there is a quantity, which might be considered as a proxy for these different processes. The relative humidity (with respect to a stable phase of water, i.e., liquid or solid) is the control variable for many cloud processes. On the other hand, this variable, as combined by the mass concentration of water vapor, pressure, and temperature, is a good indicator for adiabatic expansion processes (i.e. cooling); high values of RH can be expected if moist air is adiabatically lifted. In the tropopause region within the low temperature regime (i.e. $T < 235\,\mathrm{K}$), relative humidity over ice (RHi) is the relevant quantity, since solid ice is the stable phase there. Thus, RHi might be a good indicator for the strong lifting of air masses in baroclinic instabilities, thus working as a proxy for strong TILs.

Water vapor is a strong greenhouse gas, especially in the infrared range; the absolute concentration of water molecules controls the amount of emission and absorption. Particularly in case of a moist layer we would expect a strong emission of energy in the infrared spectrum, and thus a cooling of the layer. However, the total amount of water molecules is not the only reason for strong emissions. Since the atmosphere is layered, the concentration of water vapor in adjacent layers is also of importance. If the layers of different temperatures have a similar amount of water vapor, the emitted radiation is easily absorbed by the layers on top. Thus, a strong gradient in concentration (e.g. a layer with low concentration on top of a layer with high concentration) leads to a much stronger cooling rate than in a situation with weak gradients. Since it is difficult to measure (or determine) the gradient in water vapor concentrations, a good compromise is the use of relative humidity. Since it is linear

in the water vapor concentration, it represents the gradients in a meaningful way. Because of small temperature changes in adjacent layers with strong vapor gradients, the impact of the temperature is quite negligible. For the tropopause region, this phenomenon was investigated in a study by Fusina and Spichtinger (2010); a stronger gradient in RHi leads to a much more pronounced cooling on top of the moist layer.

In summary, the use of relative humidity over ice in the tropopause region might help to detect strong TILs. Or in other words, correlations between high values of RHi and strong TILs would corroborate the two step formation of TILs with adiabatic and diabatic components. Therefore the use of RHi is highly relevant for the investigation of the tropopause inversion layer.

The aim of this study is twofold: First, we want to demonstrate that even with the coarse resolution of ERA5 data it is possible to represent features in the tropopause region as the tropopause inversion layer (TIL) in a qualitative way. In addition, the quantitative analysis shows that the absolute values of the TIL properties as, e.g., maximum values of static stability quite closely agree with the values as obtained from high resolution data (i.e. radiosondes). Second, we want to investigate the correlation of the quantity of relative humidity with the strength of the TIL. Because of the general formation mechanisms of the TIL in terms of adiabatic (dynamic) and diabatic processes, the quantity relative humidity is the relevant variable, which is related to the formation processes of the TIL. In this study, we make the first attempt to evaluate reanalysis data on a statistical basis, generalizing the findings from case studies and idealized simulations as carried out by Kunkel et al. (2016).

For the first investigation, nearly 10,000 high-resolution radiosonde ascents from a weather station in Germany (Idar-Oberstein) are analyzed. Additionally, this investigation is combined with the ERA5 reanalysis data from the European Centre for Medium-Range Weather Forecasts (ECMWF) for the same location. This approach allows for an evaluation of the quality of ERA5 data concerning the TIL at the presented location. Given that the TIL is associated with strong gradients in stability, the comparison of model data with high-resolution measurements is indispensable.

In the second step, we investigate the correlation between relative humidity and static stability from the ERA5 data in order to corroborate the findings of Kunkel et al. (2016) in a statistical way. Upon successful assessment of data quality, we can extend our analysis to examine the TIL in a similar manner at other locations. We have focused on regions at a similar geographical latitude but with varying frequencies of baroclinic activity. This approach enables us not only to unravel seasonal differences but also to incorporate the influence of atmospheric or even regional peculiarities into the interpretation of the results.

This study is organized as follows. In Section 2 we present details on the data and methods used to identify the important quantities of TIL characteristics. Section 3 presents the results. First a comparison of measurements and reanalysis data is provided, followed by an investigation of the influence of the relative humidity on TIL properties. Finally, we extend the examination on geographical and seasonal variations. Conclusions are found in section 4.

2 Data and Methods

In this section we describe the data sets, the relevant variables, and the methods for the statistical investigations.

2.1 Data

This study is partly based on radiosonde data from a measurement site at Idar-Oberstein (Germany, 49.69° N, 7.33° E). This site was selected, because the German weather service (Deutscher Wetterdienst, DWD) provides 9 years of high resolution radiosonde data as open access. The exact used time frame spans from the 1st of January 2011 to the 31th of December 2019.

95   The radiosonde measurements are compared with the reanalysis data set ERA5 (Hersbach et al., 2020) provided by the ECMWF. After the comparison and evaluation of the data at the selected site, profiles at different geographical locations are investigated based on the ERA5 data set.

2.1.1 Radiosonde data

Idar-Oberstein is one out of 12 stations in Germany, where the DWD executes synoptic (daily at 00, 06, 12, 18 UTC) high
100   resolution radiosonde soundings. The station is located at 49.69° N and 7.33° E at 376 m altitude above sea level. For the radiosonde measurements the Vaisala RS92-SGP (01/01/2011 - 12/03/2017 & 15/06/2017 - 31/12/2019) sonde and the Vaisala RS41-SGP (28/03/2017 - 14/06/2017) sonde are used, respectively. The characteristics of the two types of radiosondes are very similar; however, the RS41-SGP has a slightly higher precision than the RS92-SGB (Vaisala, 2014). Therefore, the data is treated as if the entire data set is measured by the RS92-SGP radiosonde.

105   During one ascent of the radiosonde, the meteorological variables are measured with a time resolution of 0.5 Hertz, providing the longitude and latitude by a GPS-sensor, the geopotential height $\Phi_g\,[\mathrm{m}]$, the ambient pressure $p\,[\mathrm{hPa}]$, the temperature $T\,[\mathrm{K}]$ and the relative humidity over liquid water $\mathrm{RH}\,[\%]$, respectively. In a first approximation geopotential height Φ_g is equal to the vertical height z. For the considered data set this approximation is quite good, because of Idar-Oberstein's latitude of 49.69° N and our focus on investigations in the UTLS.

110   This investigation focuses on the upper troposphere and lower stratosphere (UTLS). For obtaining a complete and consistent data set, profiles with a maximum height lower than 20 km and profiles containing missing data are discarded. Over the period from 01/01/2011 to 31/12/2019, the data set contains 10224 single profiles. 419 profiles are discarded, 311 due to insufficient maximum height, 19 due to missing data and 89 due to unreliable values of temperature and relative humidity.

The uncertainties of the RS92-SGP regarding the measurements are given by the manufacturer (Vaisala, 2013). The tem-
115   perature sensor has a reaction time less than $2.5\,\mathrm{s}$ and a total uncertainty of $0.5\,^{\circ}\mathrm{C}$. The humidity sensor has a response time between $0.5\,\mathrm{s}$ and $20\,\mathrm{s}$ with a total uncertainty of $\mathrm{RH} = 5\,\%$. The pressure sensor has a total uncertainty of $1\,\mathrm{hPa}$ for 1080 to $100\,\mathrm{hPa}$ and $0.6\,\mathrm{hPa}$ for 100 to $3\,\mathrm{hPa}$.

The radiosonde humidity data are time-lag corrected according to Miloshevich et al. (2004) and the water vapor measurements are corrected using the algorithm and coefficients used by Miloshevich et al. (2009). Although the algorithm was
120   developed for the RS92 sonde, it can be applied to the few data points as obtained from the RS41-SGP sonde.

2.1.2 ERA5

ERA5 is the most recent reanalysis product of the ECMWF (Hersbach et al., 2020). The reanalysis is a mix of a recalculation of past weather with one fixed forecast model version (IFS CY41R2) and assimilated measurements made for each available time. The high resolution data set has a horizontal resolution $0.25°$ in longitude and latitude. The vertical dimension of the atmosphere is represented by hybrid sigma/pressure (model) levels in ERA5 (ECMWF, 2020), the number of levels is 137 of which only levels up to the lower stratosphere are used. In the tropopause region, the vertical resolution is about $300\,\text{m}$.

For the comparison with the radiosonde data we obtained pseudo-radiosonde profiles, i.e. a vertical column at a fixed grid point. The vertical profile is extracted at the grid point $49.75°$ N and $7.25°$ E, which is the closest grid point of ERA5 to the actual location of Idar-Oberstein ($49.69°$ N and $7.33°$ E). The date and the time of the extracted columns are matched with the reduced radiosonde data set to obtain a maximum of comparability between the data set. For comparison, the relevant variables, as, e.g., the geopotential height Φ_g are calculated.

2.1.3 Data gridding

In order to guarantee comparability between the radiosonde data and ERA5 it is mandatory to grid them vertically. A regular grid leads to a evenly spacing between data points, which in in turns allows for a straightforward statistical analysis. The base of the regular grid is the geometric height z.

Radiosondes use the buoyancy force to ascend, thus the vertical speed and consequently the vertical resolution is not constant. The buoyancy speed of the used radiosondes is ranging from $2\,\text{m}\,\text{s}^{-1}$ to $8\,\text{m}\,\text{s}^{-1}$ (with a mean around $5\,\text{m}\,\text{s}^{-1}$), returning a vertical resolution of 4 to $16\,\text{m}$, respectively, what is usually recognized as high-resolution data (Xu et al., 2023). The final data grid has a $30\,\text{m}$ resolution starting from station height $376\,\text{m}$ above sea level up to $20\,\text{m}$ in order to reduce the amount of unused data. The interpolation is performed with a cubic spline, which offers sufficient accuracy for this study.

By converting the ERA5 data from a pressure grid to a grid with the geometric height z, the latter grid changes from one point in time to the next with each atmospheric state. Thus, the ERA5 data set is interpolated on the same grid as the radiosondes data ($376\,\text{m}$ to $20\,\text{km}$, with $30\,\text{m}$ resolution) using a cubic spline. The ERA5 data set is heavily over-sampled with a $30\,\text{m}$ resolution, meaning the high resolution does not provide additional information; however, the choice is made in order to make the ERA5 data set comparable to the radiosonde data. Finally, we obtained comparable data sets.

2.2 Relevant variables

Since most of the desired variables are not directly available, they are calculated from the available variables in the data set. Therefore, the calculation of the relative humidity with respect to ice RHi (%), the potential temperature θ (K) and the Brunt-Väisälä-frequency N^2 (s^{-2}) are described below.

The relative humidity is defined as the ratio of the partial pressure of water vapour p_v over the saturation pressure p_s, which depends on the relevant stable phase (liquid or solid water phase). In this study, the parameterization described by Sonntag (1990) is used for the saturation pressure with respect to liquid water $p_{s,liq}$ and ice $p_{s,ice}$. This choice is motivated by the

fact that these formulae are used for radiosonde evaluations by default. The use of RHi as a variable is related to the low temperature regime in the UTLS (for $T < 240$ K, see, e.g., Reutter et al., 2020) with hexagonal ice as a stable phase of water.

155   The quantity RHi is derived from RH (relative humidity over liquid water) of the radiosonde using the following relationship:

$$RHi = RH \cdot \frac{p_{s,liq}(T)}{p_{s,ice}(T)} \tag{1}$$

Note, that the most accurate and physically sound formulations for the saturation pressure (over ice or liquid) according to Murphy and Koop (2005) deviate only slightly from the formulae above in the respective temperature regime, leading to

160   a positive bias in the resulting relative humidity over ice of a few percent, which increases with decreasing temperatures. However, for temperatures at the extratropical tropopause region, this deviation does not crucially affect the investigations.

The variable RHi constitute not only a measure for atmospheric humidity, but also serve as a good proxy for determining the relevant processes, which lead to the formation and further strengthening of the TIL: Adiabatic cooling leads to higher values of RHi, and diabatic processes as cloud formation and radiative feedbacks are also controlled by this quantity. In addition this

165   humidity variable is a linear variable (in the range between 0 and about 170%), which makes the evaluations simpler and more robust, than using the specific humidity, which in turn does not allow a relation to cloud processes without additional variables.

The ERA5 data set provides the humidity as the specific humidity q $(\text{kg}\,\text{kg}^{-1})$ which is converted to the relative humidity over ice using the following approximation:

$$\text{RHi} \approx \frac{q \cdot p}{\epsilon \cdot p_{s,ice}(T)} \tag{2}$$

170   with the ratio of the molar masses of water and air, $\epsilon = \frac{M_{\text{mol,water}}}{M_{\text{mol,air}}} \approx 0.622$.

Potential temperature θ is equivalent to the specific entropy of dry air, assuming the ideal gas approximation for dry air. It allows to compare parcels of air at different pressures levels, and, by definition, it is a conserved quantity for isentropic (i.e. adiabatic) processes. We use the common definition of θ as stated in eq. (3) with a constant specific heat capacity $c_p = 1.005\,\text{kJ}\,\text{kg}^{-1}\,\text{K}^{-1}$ of dry air:

$$175 \quad \theta = T \left(\frac{p_0}{p} \right)^{\kappa} \text{ with } \kappa = \frac{R}{c_p} \approx \frac{2}{7} \tag{3}$$

Here, $p_0 = 1000$ hPa denotes the reference pressure level, and $R = 287.05\,\text{J}\,\text{kg}^{-1}\,\text{K}^{-1}$ is the specific gas constant for air. This definition with constant c_p is accurate enough for investigations in the tropopause region (see discussion in Baumgartner et al., 2020). The relation to specific entropy of dry air is given by $ds = c_p d\log(\theta)$.

The static stability of dry air or, more commonly, the Brunt-Väisälä-frequency squared N^2 is a common measure for the

180   stability of the dry atmosphere (Hantel, 2013). $N^2 < 0$ characterises an unstable stratification, $N^2 = 0$ a neutral stratification and $N^2 > 0$ a stable stratification, respectively. The free troposphere is dominantly stable and the stratosphere is considerably more stable than the troposphere. The static stability is derived from the buoyancy force (i.e. Archimedes' principle) and can be approximate by:

$$N^2 = \frac{g}{\theta} \cdot \frac{\partial \theta}{\partial z} = \frac{g}{T}(\Gamma_d - \Gamma) \tag{4}$$

with $g = 9.8066\,\mathrm{m\,s^{-2}}$ the (mean) gravitational acceleration, $\Gamma_d = \frac{g}{c_p}$ the dry adiabatic lapse rate, and $\Gamma = \frac{\partial T}{\partial z}$ the actual temperature lapse rate based on the geometric height z, respectively.

This approximation is working under the assumption of dry air and returns on average too high values for the Brunt-Väisälä-frequency; moisture leads to strong decrease in the static stability, even if no phase change is triggered (Durran and Klemp, 1982). However, a moist, and commonly accepted, analog to dry static stability is still missing, although there are some attempts for a consistent treatment (Peters et al., 2022). Therefore we use dry static stability to ensure comparable results with literature which use the dry approximation (e.g. Gettelman and Wang, 2015; Birner et al., 2002; Birner, 2006; Erler and Wirth, 2011).

As the measurements of a radiosonde are discrete, a numerical approximation of the derivative is necessary. Since the grid increments are quite small, the numerically derived gradients are highly variable. Thus, a centered approximation of the 4th order is used

$$\frac{\partial \theta}{\partial z} \approx \frac{4}{3}\frac{\theta_{z+1} - \theta_{z-1}}{z_{z+1} - z_{z-1}} - \frac{1}{3}\frac{\theta_{z+2} - \theta_{z-2}}{z_{z+2} - z_{z-2}} \tag{5}$$

in order to smooth the resulting finite gradient approximations. However, even this high order method leads to a highly variable N^2 profile. For a better handling, the profile is additionally smoothed using a running mean with a window of 330 m, as can be seen in Fig. 1.

2.3 Calculation of tropopause characteristics

2.3.1 Definition of tropopause

The tropopause separates the troposphere and the stratosphere, constituting a transport barrier for trace gases and cloud particles. There are several attempts to define the tropopause using different approaches. We list the most common approaches; however, afterwards we will use the classical definition of a thermal tropopause, as defined by the World Meteorological Organisation (WMO) in the middle of the last century. More details about the history and difficult definition of the tropopause we refer to the studies by Hoinka (1997); Maddox and Mullendore (2018); Tinney et al. (2022) and Hoffmann and Spang (2022).

The tropopause can be defined on the basis of different variables, as e.g., physical temperature, potential temperature, potential vorticity (PV), or even chemical trace gases, as e.g. ozone. In the classical definition by the WMO (1957) the lapse rate of the temperature is taken into account. The full criterion can be stated as *"The first tropopause is defined as the lowest level at which the lapse rate decreases to 2 K per kilometer or less, provided also the average lapse rate between this level and all higher levels within 2 kilometers does not exceed 2 K"* (WMO, 1957). For the tropics, sometimes the so-called cold point temperature is used, i.e. the first minimum in the free troposphere of the physical temperature (Highwood and Hoskins, 1998).

In a further step, the potential temperature θ can be used as a basis variable. The gradient of θ can be used as a simple measure for the static stability, thus influencing tracer transport (see, e.g., Kunz et al., 2011). The tropopause can be defined
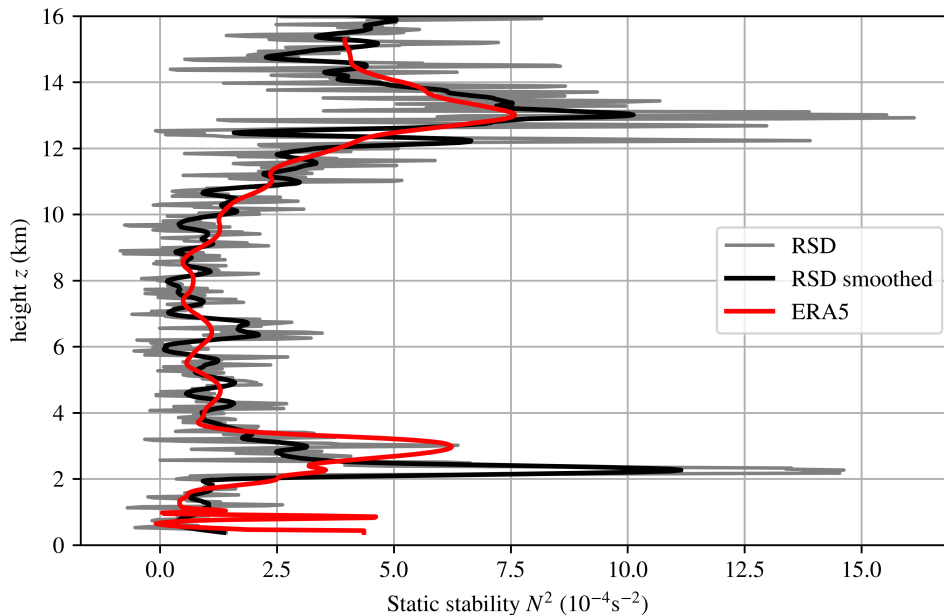
Figure 1. Example of a static stability profile from the 02.01.2011 0 UTC with (grey) the calculated N^2 from radiosonde data, (black) the $330\,\mathrm{m}$ window smoothed N^2 from radiosonde data and (red) the calculated N^2 from ERA5 data.

as the height level at which a certain threshold in the gradient $\frac{\partial \theta}{\partial z}$ exceeds a certain threshold (e.g. $\frac{\partial \theta}{\partial z}\big|_{\mathrm{thres}} \sim 0.012\,\mathrm{K\,m^{-1}}$,

215   see Mullendore et al., 2005). Following the discussion by Tinney et al. (2022), it seems that a refined version of this definition might be most robust. From the potential temperature, the Brunt-Väisälä (or buoyancy) frequency can be calculated, see eq. (4). Instead of using the Brunt-Väisälä frequency itself, Birner (2010) introduced the level of the maximum gradient of N^2 as the tropopause; actually, this is the level of the maximum curvature of the temperature, which can be set in relation to the residual circulation.

220   From an atmospheric dynamics perspective, the potential vorticity as an adiabatic invariant is investigated. The level of a certain (but kind of arbitrary) threshold is the set as dynamical tropopause. While often the threshold of 2 PVU is used, Kunz et al. (2011) showed that the value in terms of transport barriers can vary between 1.5 and 5 PVU, also depending on the season. The threshold of 3.5 PVU often produces a dynamical tropopause height, which is close to the thermal tropopause level as derived by WMO criterion (Hoerling et al., 1991).

225   Finally, chemical trace gases are used to define the tropopause as a transport layer. Actually, from this point of view the tropopause is not an ideal clear defined interface between troposphere and stratosphere, but merely a transition layer (see, e.g., discussion in Gettelman et al., 2011). The depth of the transition layer was investigated using tracer-tracer correlation, e.g. using ozone and carbon monoxide (Pan et al., 2004). Since there is a clear signal in the ozone concentration in the different vertical layers (troposphere vs. stratosphere), a threshold criterion might be used to define the ozonopause, which should be

230 close to tropopause levels derived from other definitions. Bethan et al. (1996) used a threshold of ozone mixing ratio in order of 100-110 ppb and showed that the ozonopause is usually quite close to the thermal tropopause. This approach was used further for a simple discrimination of aircraft data (see, e.g., Gierens et al., 1999) and for other applications without using a full 3D data set of meteorological variables. In some investigations, the hygropause (i.e. the minimum in water vapor concentrations) was also used as a proxy. However, this approach is not really successfully applied for data analysis. Although there might be

235 more modern definitions of the tropopause level, we stick with the classical definition by WMO (1957). This is mostly due to a better comparison with former studies on the tropopause inversion layer (e.g. Birner et al., 2002; Birner, 2006); however, this definition represents the nature of the transport barrier very well and is still a standard definition for the daily reports of all weather services in the world.

One should keep in mind that almost all definitions of the tropopause level were driven by the large scale perspective of

240 atmospheric dynamics, i.e. using the viewpoint that the vertical change in the thermodynamic variables (i.e. temperature and pressure, respectively) is smooth enough. This viewpoint is clearly represented in the WMO definition using lapse rates, where changes over a long vertical extent are investigated. In general, this definition requires a certain vertical resolution, whereas deviations in both directions might raise issues. For very coarse resolution data as in low resolution radiosonde reports, former reanalysis data or climate models, the determination of lapse rates causes problems, which can be handled with some refined

245 methods (see, e.g., Hoinka, 1998; Reichler et al., 2003).

For high resolution data, as in operational radiosondes or partly in the new generation of reanalysis data (see, e.g., a similar discussion about front detection in Niebler et al., 2022), the variables are not smooth enough for the determination of gradients; actually, the high resolution leads to strong variations or even nonphysical noise. In extreme cases, the WMO criterion is never fulfilled, since the lapse rate is crucially changing within the required extension of $2\,\mathrm{km}$, see also discussion in Maddox and

250 Mullendore (2018). For high resolution data, averaging (e.g. running means) of high resolution data or higher order finite difference methods for determining the gradients can be applied, see, e.g., the calculation of $\frac{\partial \theta}{\partial z}$ in eq. (5). However, the question remains if the definition of a tropopause layer as driven by the large scale viewpoint of atmospheric dynamicists is still meaningful, if we consider much smaller scales. At least for investigations of convective events, some effort is made to find more robust measures for the tropopause characteristics (see, e.g., Tinney et al., 2022).

255 ### 2.3.2 Relative coordinates

In order to be able to compare the large number of radisonde data and ERA5 profiles, a tropopause-centered coordinate system was introduced. For this purpose, the thermal tropopause is identified in each radiosonde and ERA5 profile for Idar-Oberstein and defined as the tropopause height TP_z. This means that all profiles now live in the same coordinate system and can be averaged to obtain mean profiles of temperature, humidity and static stability. Therefore. we introduce a new height variable

260 $$z_{TP} = z - TP_z \qquad (6)$$

relative to the tropopause height TP_z (as derived by the WMO criterion, see above). Negative altitude values z_{TP} denote the upper troposphere, whereas positive altitude values z_{TP} represent the lower stratosphere. For the averaging process the single
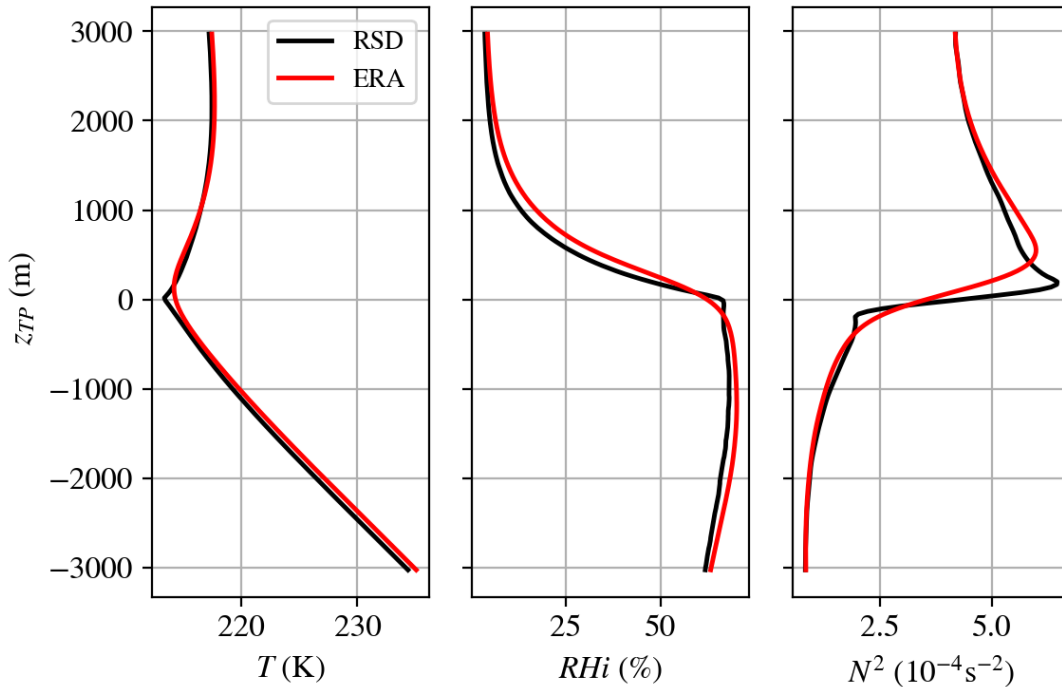
Figure 2. The average vertical profile in the tropopause relative height z_{TP} coordinate system of temperature T, relative humidity over ice RHi and static stability N^2 for the radiosondes (black) and ERA5 (red).

profiles are transformed into the z_{TP} coordinate system and the arithmetic mean of a meteorological variable $\chi \in \{\text{temperature, relative humidity, static stability}\}$ is calculated, summing over all profiles at a certain height.

265   The mean profiles relative to tropopause height of temperature, static stability (N^2), and RHi can be seen in Figure 2 for the radiosonde measurements (black) and the corresponding ERA5 data set (red) at the location of Idar-Oberstein. Even for the mean profiles the characteristics of the TIL, i.e., the strong increase in N^2 at around TP_z can be seen clearly, as described in the next section. However, Figure 2 also shows that the results differ between radiosonde and reanalysis data. In the temperature profile of ERA5, the minimum temperature is less pronounced, as well as the values in RHi at the tropopause level. The static

270   stability profile shows a deviation of the maximum in N^2, i.e. the level of the maximum is shifted towards higher altitudes and the maximum is less pronounced as compared to the high resolution radiosonde data. These differences are mainly based on the vertical resolution of the data sets, which is significantly lower in the case of the ERA5 data than in the radiosonde data. As a result, sharp gradients cannot be resolved as good, as can be seen in particular when looking at N^2. A detailed comparison between the radiosonde and ERA5 data can be found in Section 3.1.1.
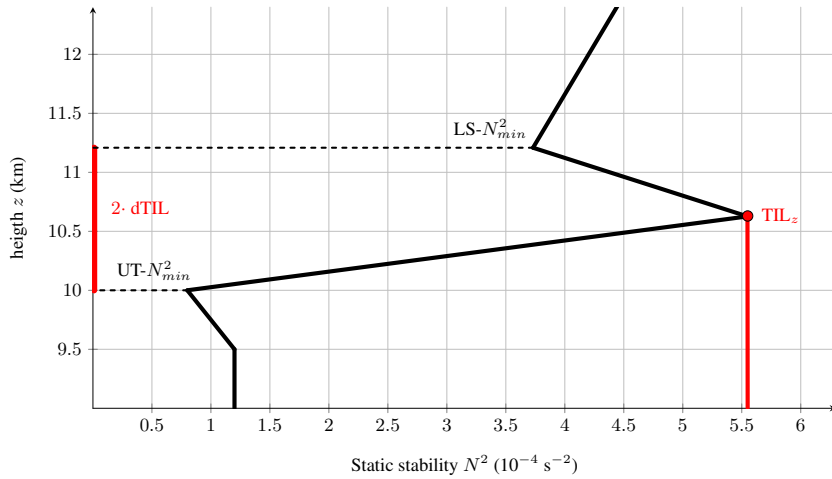
Figure 3. A schematic drawing of the different diagnostics of the tropopause inversion layer, i.e. the TIL depth dTIL and the strength of the TIL, sTIL, respectively. These features (minima and maximum in N^2) can also be seen in the realistic profile represented in figure 1.

2.3.3 Tropopause inversion layer

The tropopause inversion layer (TIL) is a region of extraordinary high static stability within the tropopause region and was found by averaging vertical profiles with respect to the tropopause level. The TIL is also present in single vertical profiles of radiosondes (Birner et al., 2002) and models (Birner, 2006). The high stability in the TIL region represents a barrier to vertical motion (Gettelman et al., 2011) and is therefore important for understanding the composition of the air in the upper troposphere and lower stratosphere. Although there are investigations of the TIL properties since more than two decades, a clear (or even common) definition of the TIL and its main features (as e.g. strength) is missing. For this study, we define the TIL strength **sTIL** as the maximum of the static stability N^2_{max} within $3\,\text{km}$ above tropopause level and the altitude level of N^2_{max} as the TIL height TIL_z. Two additional heights are defined through two minimum values of N^2: UT-N^2_{min} is the height of the minimum of N^2 in the upper troposphere, and LS-N^2_{min} is the height of the minimum of N^2 within $5\,\text{km}$ above TIL height. The TIL depth **dTIL** is half of the height difference between the UT-N^2_{min} and LS-N^2_{min}. The diagnostics of the TIL with the main features and the newly introduced quantities sTIL and dTIL are summarized in Figure 3. If one of the features such as UT-N^2_{min} or LS-N^2_{min} could not be determined, these profiles were excluded from consideration in this study. This affected 126 profiles, so that in the end 9678 profiles were included in the analysis in this study. Note, that the real profile of high resolution data (radiosonde and ERA5) as represented in Figure 1 includes all the features of the scheme shown in Figure 3 (UT minimum of N^2, maximum of N^2, LS minimum of N^2). After averaging over many tropopause-centered profiles, some features might be lost in the mean profiles (e.g. Figure 2), although they are still visible in the single profiles – otherwise the profiles would be discharged in the analysis.

2.3.4 Calculation of humidity measure

The analysis of the humidity of the upper troposphere and the lower stratosphere is based on the average humidity with respect to ice below the TIL, denoted by wRHi. It is calculated by averaging RHi from the height of the $500\,\text{hPa}$ pressure surface z_{p500} up to the TIL level TIL_z, as defined in (7).

$$\text{wRHi} = \frac{1}{\text{TIL}_z - z_{p500}} \int\limits_{z_{p500}}^{\text{TIL}_z} \text{RHi}(z)\, dz \approx \frac{1}{\text{TIL}_z - z_{p500}} \sum_{z=z_{p500}}^{\text{TIL}_z} \text{RHi(z)}\, \Delta z \tag{7}$$

This moisture (or humidity) is used in the further course to sort the vertical profiles according to different moisture contents.

3 Results

Based on the spatially and temporally highly resolved ERA5 data, the properties of the tropopause region related to the static stability and relative humidity in this region are investigated in more detail. As stated in the motivation, our goal of this study is twofold. First, we want to show that there is good agreement of high resolution radiosondes and ERA5 data in terms of representing the main features of TILs in the extratropics. Therefore, the measured data of the radiosondes are compared with the corresponding data of the reanalysis model. Second, we want to show that relative humidity is the key quantity for TILs, thus there is a strong correlation between high humidity measures and sharp/strong TILs. This is investigated in more detail, also with the consideration of seasonal and geographical differences.

3.1 TIL properties in measurements and reanalysis data

A very good agreement between the radiosonde measurements and the reanalysis data is the basic prerequisite for further investigations based on the ERA5 data. Therefore, in a first step, the deviations between radiosonde measurements and reanalysis data for the variables temperature T, relative humidity with respect to ice RHi and static stability N^2 are investigated. In the next step, the results for the different heights (TP_z, TIL_z) are investigated. Finally, the TIL properties such as TIL thickness and TIL depth are compared.

3.1.1 Comparision of temperature, relative humidity with respect to ice

The deviation between radiosonde measurements and ERA5 data in a variable χ are quantified by the average measure $\overline{D}_{\text{abs}}(\chi)$ for every single profile. This quantity can be calculated as follows:

$$\overline{D}_{\text{abs}}(\chi) := \frac{1}{z' - z_0} \int\limits_{z_0}^{z'} |E(\chi) - R(\chi)| \mathrm{d}z \approx \frac{1}{z' - z_0} \sum_{z_0}^{z'} |E(\chi(z)) - R(\chi(z))| \Delta z \tag{8}$$

with z_0 the start and z' the end height of the averaging, χ the meteorological variable of interest, E, the ERA5 profile and R the radionsonde profile, respectively. Δz is the height difference between two adjacent levels. We chose a metric including

absolute values of differences in order to avoid undesired cancellation effects of positive and negative contributions. In this sense, we used a metric inspired by the L_1-norm. Thus, the resulting distributions are expected to be skew and might have (exponential) decaying tails. The resulting data set is visualised in a probability bar chart and the corresponding median, mean and standard deviation for the different variables are presented in figures 4, 5, and 6, respectively.

(a) Upper troposphere UT
(b) Lower stratosphere LS
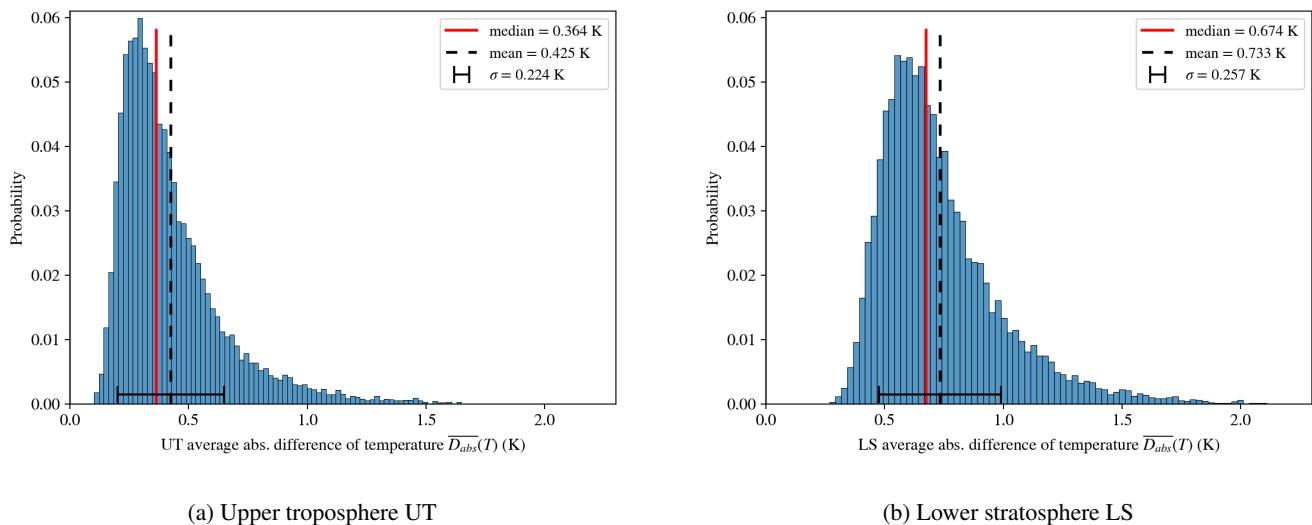
Figure 4. Probability distribution of average difference of temperature $\overline{D}(T)$ between ERA5 and radiosondes for upper troposphere UT (a) and the lower stratosphere LS (b). The median is displayed in red, the mean is represented by a dashed black line and standard deviation σ is represented as error bar.

The temperature deviations between the radiosondes and ERA5 for the upper troposphere ($z_0 = -3000\,\text{m}$, $z' = 0\,\text{m}$, Fig. 4a) show a skew distribution with a median of $0.37\,\text{K}$, a mean of $0.43\,\text{K}$ and a standard deviation $\sigma = 0.22\,\text{K}$. For the lower stratosphere ($z_0 = 0\,\text{m}$, $z' = 3000\,\text{m}$) the distribution of the temperature deviation is similar (4b). However, the median ($0.67\,\text{K}$) and mean ($0.73\,\text{K}$) values are significantly larger, with a standard deviation of $\sigma = 0.26\,\text{K}$. Generally we know that ERA5 has on average slightly warmer temperatures compared to the measurements. In order to interpret these results, it should be mentioned that the measurements have an uncertainty of $0.5\,\text{K}$ according to the manufacturer (Vaisala, 2013).

For deriving a robust statement about the humidity impact on the TIL in the tropopause region, the relative humidity with respect to ice (RHi) is used. As mentioned above, this is the key thermodynamic control variable for ice cloud processes, thus determining also the life cycle of ice clouds. The consistency of the moisture data is also important for the description of the average relative humidity with respect to ice wRHi. The distributions in Figure 5 for mean differences show a shift to higher deviations of RHi in ERA5. This behavior is due to the fact that ERA5 data does not capture the moisture gradients at the tropopause as sharply as the radiosonde data. The humidity features, i.e. the fine structures, are smeared out; this is partly due to the coarse vertical resolution of the ERA5 data but probably also due to issues in the data assimilation of moisture in cold temperature regimes. This difference dominates the value of $\overline{D}_{\text{abs}}(\chi)$ for each individual vertical profile; thus, we would expect
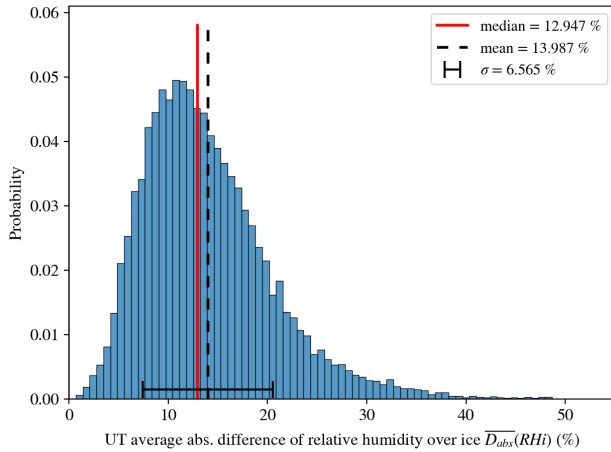
(a) Upper troposphere UT
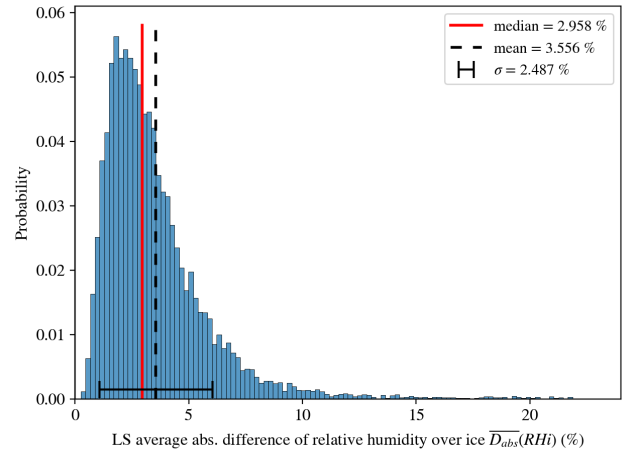
(b) Lower stratosphere LS

Figure 5. Probability distribution of average difference of relative humidity over ice $\overline{D}(\mathrm{RHi})$ between ERA5 and radiosondes for upper troposphere UT (a) and the lower stratosphere LS. With the median in red, the mean in dashed black and standard deviation σ as error bar.

less steep gradients for RHi in the ERA5 data. These differences are again distributed with some skewness, leading to quite similar median value ($12.95\,\%$) and mean value ($13.99\,\%$) in the upper troposphere, and accordingly to median value ($2.96\,\%$) and mean value ($3.56\,\%$) in the lower stratosphere. The standard deviation for the upper troposphere is $\sigma = 6.57\,\%$ which is

340   a considerable deviation, where relative humidity over ice ranges from 0% - 105%. In the lower stratosphere, where relative humidity is generally much lower than in the troposphere, the standard deviation is $\sigma = 2.49\,\%$.

     The static stability or Brunt-Väisälä-frequency squared N^2 represents the main criterion to identify the tropopause inversion layer and its characteristics. Looking at the probability distribution (Fig. 6), there exists a notable difference between the upper troposphere and the lower stratosphere. In the upper troposphere (Fig. 6a), ERA5 has a tendency to be more stable with a

345   mean $= 0.40 \times 10^{-4}\,\mathrm{s}^{-2}$ and a median $= 0.43 \times 10^{-4}\,\mathrm{s}^{-2}$. The distribution is skewed towards smaller average difference values of N^2 with a standard deviation of $\sigma = 0.15 \times 10^{-4}\,\mathrm{s}^{-2}$ When comparing the average differences and the standard deviation of N^2 to the static stability for the upper troposphere $1.2 \times 10^{-4}\,\mathrm{s}^{-2}$ (Hoskins and James, 2014), the static stability is represented well in the ERA5 reanalysis.

     In the lower stratosphere (Fig. 6b), ERA5 is less stable compared to the radiosonde data with a mean $= 1.02 \times 10^{-4}\,\mathrm{s}^{-2}$

350   and a median $= 1.07 \times 10^{-4}\,\mathrm{s}^{-2}$ with tendency to smaller absolute values of static stability; the standard deviation is $\sigma = 0.31 \times 10^{-4}\,\mathrm{s}^{-2}$

     The reason for the lower stability in the lower stratosphere in ERA5 is the tropopause inversion layer, which arises through a strong gradient of potential temperature. Due to the lower vertical resolution of ERA5, strong gradients in the variables are less pronounced, leading smaller values of static stability thus resulting in a less stable vertical profile in the lower stratosphere.

355   Nonetheless, the average difference of $\sim 10^{-4}\,\mathrm{s}^{-2}$ is small compared to the average value of N^2 of $4 \times 10^{-4}\,\mathrm{s}^{-2}$.
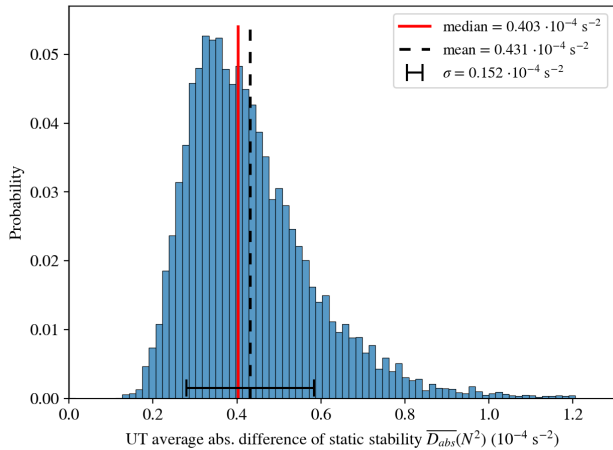
(a) Upper troposphere UT
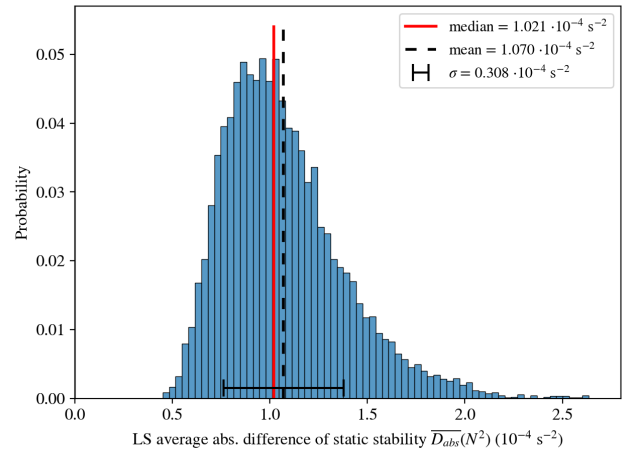
(b) Lower stratosphere LS

Figure 6. Probability distribution of average difference of static stability $\overline{D}(N^2)$ between ERA5 and radiosondes for upper troposphere UT (a) and the lower stratosphere LS. With the median in red, the mean in dashed black and standard deviation σ as error bar.

Table 1. Values of sTIL for the three different classes (low/medium/high) in the radiosonde data set and the ERA5 data set

sTIL	low	medium	high
RS	$< 6.8 \times 10^{-4}\,\mathrm{s}^{-2}$	$[6.8 \times 10^{-4}\,\mathrm{s}^{-2}, 11.2 \times 10^{-4}\,\mathrm{s}^{-2}]$	$> 11.2 \times 10^{-4}\,\mathrm{s}^{-2}$
ERA5	$< 5.2 \times 10^{-4}\,\mathrm{s}^{-2}$	$[5.2 \times 10^{-4}\,\mathrm{s}^{-2}, 8.4 \times 10^{-4}\,\mathrm{s}^{-2}]$	$> 8.4 \times 10^{-4}\,\mathrm{s}^{-2}$

Overall, we can state that the quantitative agreement between the high resolution radiosonde data and the ERA5 data is high enough to represent the profiles of T, RHi, and N^2 in a satisfying way. However, the more important issue in the comparison is the qualitative representation of TIL features in both data sets, as will be investigated in the next section.

3.2 TIL properties and humidity

360 In the following sections we investigate the relationship between TIL properties and moisture, especially in terms of TIL strength and thickness. As a measure for humidity we use the averaged relative humidity with respect to ice (wRHi) as introduced earlier in equation 7.

3.2.1 TIL strength and humidity

First, we classify the vertical profiles into tropopause inversion layers of different strengths (sTIL). The classification of sTIL

365 is based on three classes, i.e. low, medium, and high values of sTIL, with different intervals for the radiosonde data and the
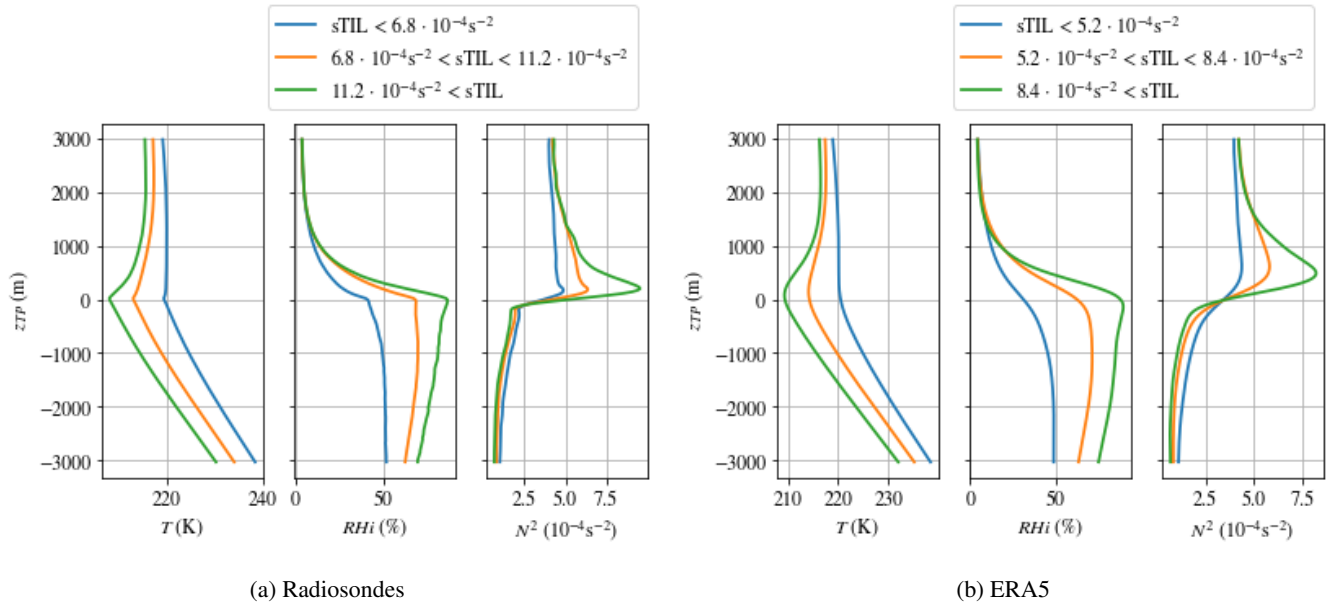
Figure 7. The mean vertical profiles for radiosondes RSD (a) and ERA5 (b) of temperature T, relative humidity over ice RHi and static stability N^2 in the tropopause relative height z_{TP}. The mean profiles are classified in terms of tropopause inversion layer strength sTIL. Colors indicate the different sTIL categories. blue: low sTIL value category, orange: medium sTIL value category, green: high sTIL value category. The exact boundary values of the categories are found in the respective legend.

ERA5 data, respectively. The ranges are represented in Table 1. The classification criteria were chosen such that one third of the vertical profiles fall into each category (low, medium, high). Since the distributions of metrics between ERA5 and radiosondes differ, the exact values of the classification boundaries are also different. Figure 7 shows the corresponding mean profiles for temperature, RHi, and static stability for the radiosondes (left) and the reanalysis data (right).

370 As expected the ERA5 reanalysis is not able to capture the sharp gradients as well as the high resolution radiosondes. This is noticeable with the sharp kinks in temperature T and relative humidity with respect to ice RHi at tropopause level (z_{TP} = 0 m) and the sharp spikes in the static stability N^2, which are present in the radiosonde data, but are smoothed out in the ERA5 data. Despite of these issues related to the resolution of ERA5, the reanalysis data show the same qualitative behaviour for temperature and RHi, respectively. Thus, the ERA5 data set can be used consistently for the investigation of TIL in the
375 extratropics.

 With the focus on the temperature profile, stronger TILs seem to be correlated with colder temperatures and thus possibly with higher tropopause heights. However, this interpretation is somewhat problematic, since warmer and colder profiles with higher and lower tropopause heights are compared. Some altitude shifts in the profiles might weakening or even cancel out these effects. The correlation between a sharper temperature inversion above the tropopause and a stronger TIL is certainly
380 expected, because the TIL strength is derived directly from the temperature gradients (Eq. 4).

Table 2. Maxima in N^2 for the different classes of wRHi as represented in figure 8

$N^2_{\max}$	low wRHi	medium wRHi	high wRHi
RS	$7.3 \times 10^{-4}\,\mathrm{s}^{-2}$	$8.2 \times 10^{-4}\,\mathrm{s}^{-2}$	$9.3 \times 10^{-4}\,\mathrm{s}^{-2}$
ERA5	$5.7 \times 10^{-4}\,\mathrm{s}^{-2}$	$6.5 \times 10^{-4}\,\mathrm{s}^{-2}$	$7.0 \times 10^{-4}\,\mathrm{s}^{-2}$

Thus, we shift our investigations to the connection between relative humidity and TIL strength. Here, we find two robust features, which can be clearly seen in the different classes of the TIL strength sTIL. For the class with the highest sTIL values (green line in Figure. 7) we find enhanced values of RHi throughout the troposphere until the tropopause level; here, the averaged values of RHi are usually above 70%. For the medium class, the relative humidity values show averaged values of about 60%, whereas in the low sTIL class, the relative humidity values are around 50%. The signal is the same for radiosonde data and ERA5 data, with slight changes in the values.

In addition, we find that for the high sTIL class the RHi gradient on top of the moist layer is much sharper than for the other two classes. Again, we see a clear decrease in the RHi gradient for the medium and low sTIL classes, respectively.

In summary, we find a sharper or stronger TIL for

1. higher RHI values in the troposphere, and

2. sharper gradients in RHi on top of the moist layer (at the tropopause height and above).

The first feature of enhanced RHi values (with a slight increase with height towards the tropopause level) can be interpreted as a signal of the adiabatic processes (e.g. during baroclinic instability evolution) enforcing a vertical upward motion (with compressing isentropes) and thus an increase in RHi. A higher value of RHi might also indicate a stronger (or even longer) adiabatic process. The second feature of a strong moisture gradient at the tropopause level might point to diabatic processes leading to irreversible foramtion of the TIL. Actually, Fusina and Spichtinger (2010) could show that the strongest radiative cooling in moist tropopause layers was triggered for strong RHi gradients. Thus, the variable RHi points to both processes according to higher values and steeper gradients, respectively.

Another way to investigate the relationship between humidity and TIL strength is to look at the sTIL distribution as a function of the mean RHi. For this purpose, the sTIL data of the radiosondes and of ERA5 were divided into three RHi classes: low wRHi (wRHi $\leq$ 45 %), medium wRHi (45 % < wRHi $\leq$ 70 %) and high wRHi (70 % <wRHi), respectively. These distributions are represented in Fig. 8, for radiosonde data (left panel) and ERA5 data (right panel), respectively.

We find in Fig. 8 that the probability density function (PDF) of the TIL strength is correlated with higher values of averaged relative humidity with respect to ice (wRHi). This is deducible by the shift of the PDF curve to higher sTIL values with higher wRHi categories. This shift is most obvious at the position of the maximum of the mode of the PDF, as can be seen in both data sets, the high resolution radiosonde data (Fig. 8a), and the ERA5 data (Fig. 8b), respectively. The values of the maximum of the modes for the different categories is listed in Table 2. It is important to mention that the PDF broadens with higher wRHi,

(a) radiosondes   (b) ERA5
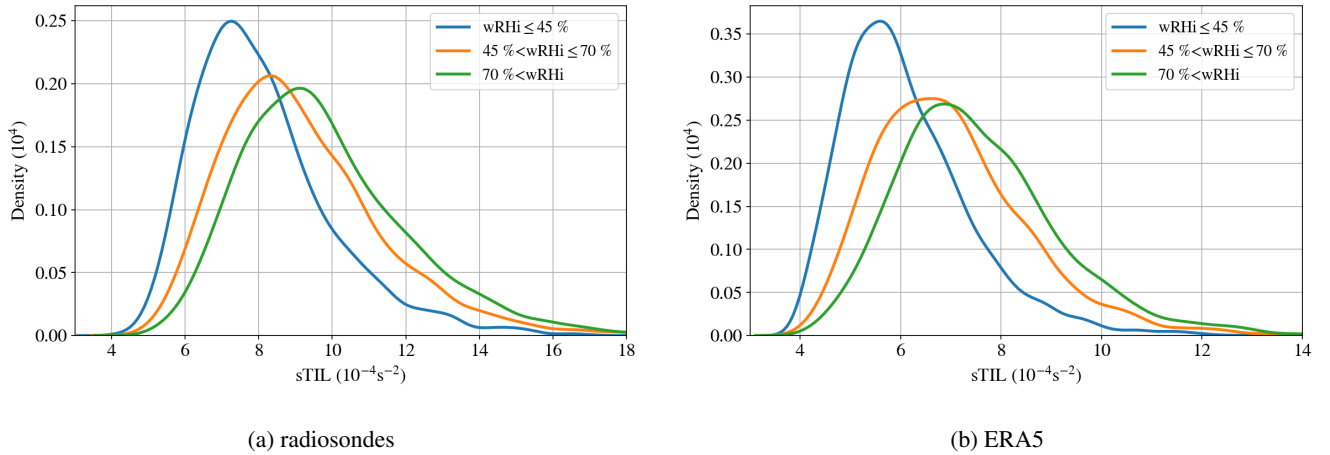
Figure 8. The probability density function for the radiosondes RSD (a) and ERA5 (b) of the TIL strength sTIL for categories of the average relative humidity over ice wRHi. Colors indicate the different categories with respect to wRHi. blue: low category (wRHi $\leq$ 45 %), orange: medium category (45 % < wRHi $\leq$ 70 %), green: high category (70 % < wRHi). Note the slightly different scale in the sTIL axis in both parts

which means that the variance of the sTIL values increases. The increased variance does not lead to the different PDF to cross in the left tail of the function, meaning that weak sTIL always have a higher probability to be in the lower humidity category. Similarly higher sTIL values ($> 9.3 \times 10^{-4}\,\text{s}^{-2}$ for radiosondes and $> 6.5 \times 10^{-4}\,\text{s}^{-2}$ for ERA5) have a higher probability of being part of the higher wRHi category.

When comparing the radiosondes (Fig. 8a) and ERA5 (Fig. 8b) the similar shape in the probability density and the same trends are apparent, while the values of sTIL are shifted to lower values when comparing ERA5 with the radiosondes.

Again we find the same qualitative behaviour for RS data and reanalysis data, although the quantitative values differ due to the different vertical resolution of the data. Overall, we can state that there is a strong indication that high RHi values are physically connected with strong TILs (via the relevant adiabatic and diabatic processes).

3.2.2 TIL depth and humidity

In addition to the strength of the TIL, we show in Fig. 9 distributions of the TIL depths dTIL distributed into different classes of averaged relative humidity with respect to ice wRHi. Here, the depth of the TIL also shows a correlation with the RHi, which is discussed in this section. The total width of the distribution does not change, so the depth of the TIL is always in the range between some few hundreds metres up to about 6000 m; however, the maximum of the distribution shows a clear deviation. As the average relative humidity over ice wRHi increases, the TIL depth dTIL is shifted to lower values.

The probability density function shows a formation of a second mode, as found in the ERA5 data set for all wRHi classes (Fig. 9b), as well as in the low wRHi category of the measurements (blue line, Fig. 9a). This formation of a double mode is
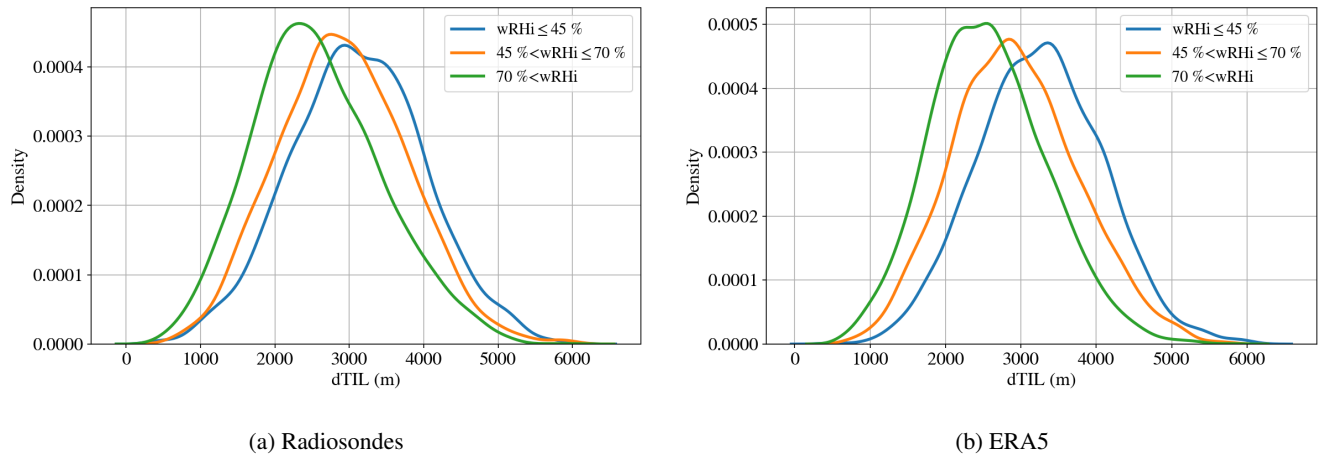
Figure 9. Probability density distribution for the radiosondes RSD (a) and ERA5 (b) of the tropopause inversion layer depth dTIL for categories of average relative humidity over ice wRHi. The low category (wRHi ≤ 45 %) in blue, the medium category (45 % < wRHi ≤ 70 %) in orange and the high category (70 % < wRHi) in green.

425   an artefact of the categorization process, in which the aim was to ensure that one third of the data per category was included. These double modes are therefore not of a physical nature. The origin is a fluctuation in the distribution, which is cut off by the boundaries of the categorisation. The artifact makes the interpretation of the mode difficult. Nonetheless there is a clear correlation between higher dTIL values and lower wRHi values . The variance of the data within each wRHi category is about the same, seen by the similar width and height of the PDF.

430   Despite the different resolutions of the underlying data, the results between ERA5 and the radiosonde data are very similar. The maximum of the distributions for the high wRHi category is approximately $2250\,\text{m}$ in both cases. In contrast, the thickness of the TIL in the driest category low wRHi is around $3000\,\text{m}$. The category in the middle with wRHI between $45\,\%$ and $70\,\%$ is about $2900\,\text{m}$ in both data sets. As mentioned above, the double mode makes exact quantification difficult.

     In summary, it can be seen that the drier the air is in this region, the thicker the TIL is. In other words, a moist upper
435 troposphere coincides with a decreased depth of the TIL. In combination with the findings from the section before, we can conclude, that for a more humid upper troposphere, we can find a stronger but vertically more confined TIL feature. This confinement might be driven by radiative processes, since a sharp moisture gradient at the tropopause level leads to a strong but vertically very confined radiative effect (see, e.g., figure 9 in Fusina and Spichtinger, 2010). In addition, a strong vertical upward motion as triggered by adiabatic processes might also lead to a confinement of the vertical TIL features. However, a
440 clear attribution of this connection is not possible, although the enhanced humidity points again to the adiabatic and diabatic processes.

3.3 Geographical variations

We found a correlation between TIL characteristics and humidity for the Idar-Oberstein site in Central Europe with radiosonde measurements and reanalysis data; thus, the next step is to investigate three additional regions representative for northern hemisphere extratropics at a similar latitude with different meteorological conditions but at different longitudes. Here, we address the question whether similar correlations can be found there, although the meteorological situation might be different in terms of large scale dynamics, i.e. in terms of developing baroclinic instabilities or evolving frontal systems. For this purpose, solely the reanalysis data are now used because of lack of high resolution radiosonde data with acceptable measurement quality for humidity variables.

Idar-Oberstein (Central Europe, C.E., 49.69°N and 7.33°E), which has already been highlighted in detail, has a low cyclone frequency with its maximum in the spring months MAM. The second location is in central Asia (C.A., 49.75°N and 87.25°E) with almost no cyclonic activity throughout the year. The third location is in central USA (USA, 42.50°N and -86.5°E), where the cyclonic frequency for the region is high in winter DJF and spring MAM, and low in summer JJA and autumn SON. The fourth location is in the North Pacific N.P. (49.75°N and -172.75°E), with very high cyclonic frequency through out the year except for a strong minimum in summer (Wernli and Schwierz, 2006).

As already investigated for the Central Europe region (Figure 8), the TIL strength is also distributed into the different moisture classes for the other locations. The results are presented in Figure 10 and confirm that the sTIL values tend to be higher when the average relative humidity with respect to ice is also high for the other regions. Also, the variability of sTIL is increasing with increased humidity in all regions. However, it is visible that the different regions exhibit different distribution shapes of the TIL strength. For example the central USA is showing the highest variability of the sTIL and the highest probability of strong sTIL events. On the contrary central Asia is showing the lowest variability and the lowest probability of strong sTIL events.

To summarize, the co-occurrence of high values of humidity with strong values for sTIL is a robust feature of the extratropics. The higher the averaged humidity is, the stronger is the resulting TIL.

3.4 Seasonal variations

This section deals with the seasonal variation of the tropopause inversion layer, which is also discussed in the literature. It was found that the interplay of water vapor on the static stability in the UTLS region occurs on seasonal time scales (Kunz et al., 2009; Hegglin et al., 2009).

3.4.1 Seasonal mean vertical profiles

Starting with the temperature profile for central Europe (Fig. 11a) the highest temperatures in the stratosphere and troposphere are found in the summer months; similarly the lowest temperatures are found in the winter months. The autumn and spring months show similar temperatures in the troposphere and at tropopause level, but significantly differ in the stratosphere with
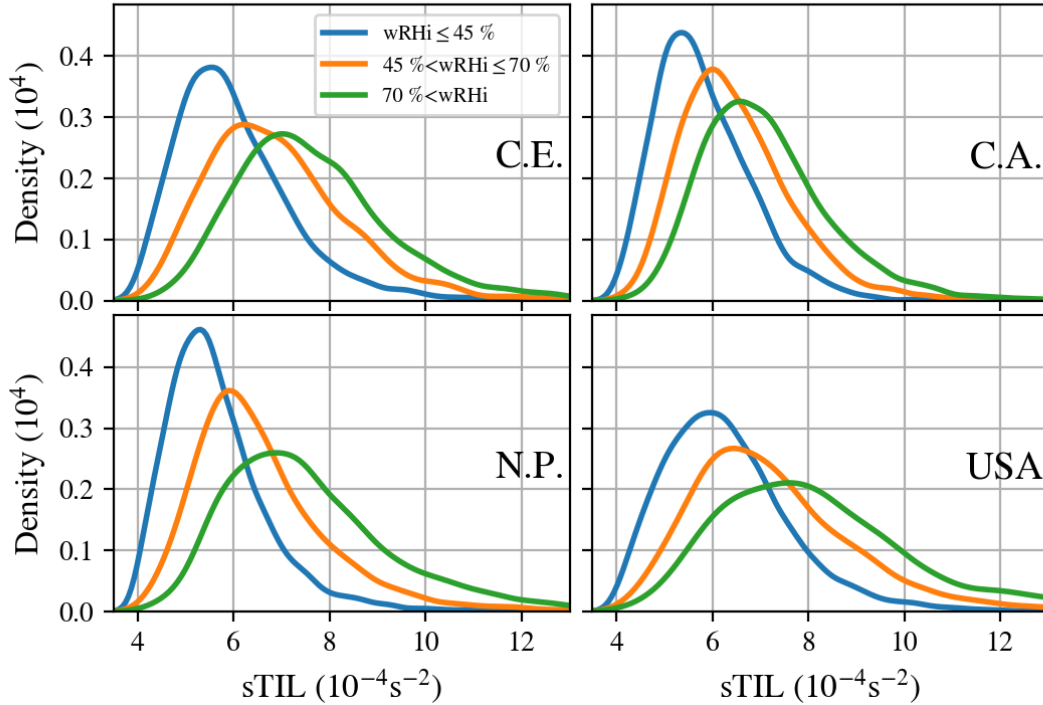
Figure 10. The probability density function of the TIL strength sTIL for average relative humidity categories. Central Europe C.E. (upper left), central Asia C.A. (upper right), the Northern Pacific N.P. (lower left) and the central USA (lower right).

autumn temperatures being colder than spring temperatures. For higher levels, the autumn temperatures match the winter temperatures.

475   The averaged RHi for central Europe on average show little seasonal difference in the troposphere. The most pronounced seasonal differences are found in the first kilometer above the tropopause. Based on the previous findings in section 3.2.1, it is expected that the spring and summer months show the strongest TIL (high sTIL values) and the thinnest TIL (low dTIL values).

    The static stability profiles show a peak of high static stability above the tropopause of similar magnitude $N^2 = 6 \times 10^{-4}\,\text{s}^{-1}$

480 across every season, with a significant difference in static stability above . Within the first 3 km above the tropopause the static stability is on average $0.48 \times 10^{-4}\,\text{s}^{-1}$ in spring compared to autumn and $0.22 \times 10^{-4}\,\text{s}^{-1}$ higher in winter compared to summer, confirming previous findings by Schmidt et al. (2010) for the extratropic region (40 °N - 60 °N). The vertical profiles over central Asia (C.A.) (Fig. 11b) show weak seasonal differences for RHi and the static stability. The summer and autumn months show slightly higher RHi below the tropopause. In contrast the temperature profiles show a high variability throughout

485 the year with the highest temperatures in summer, the lowest temperature in winter.

(a) central Europe

(b) central Asia

(c) Northern Pacific

(d) central USA
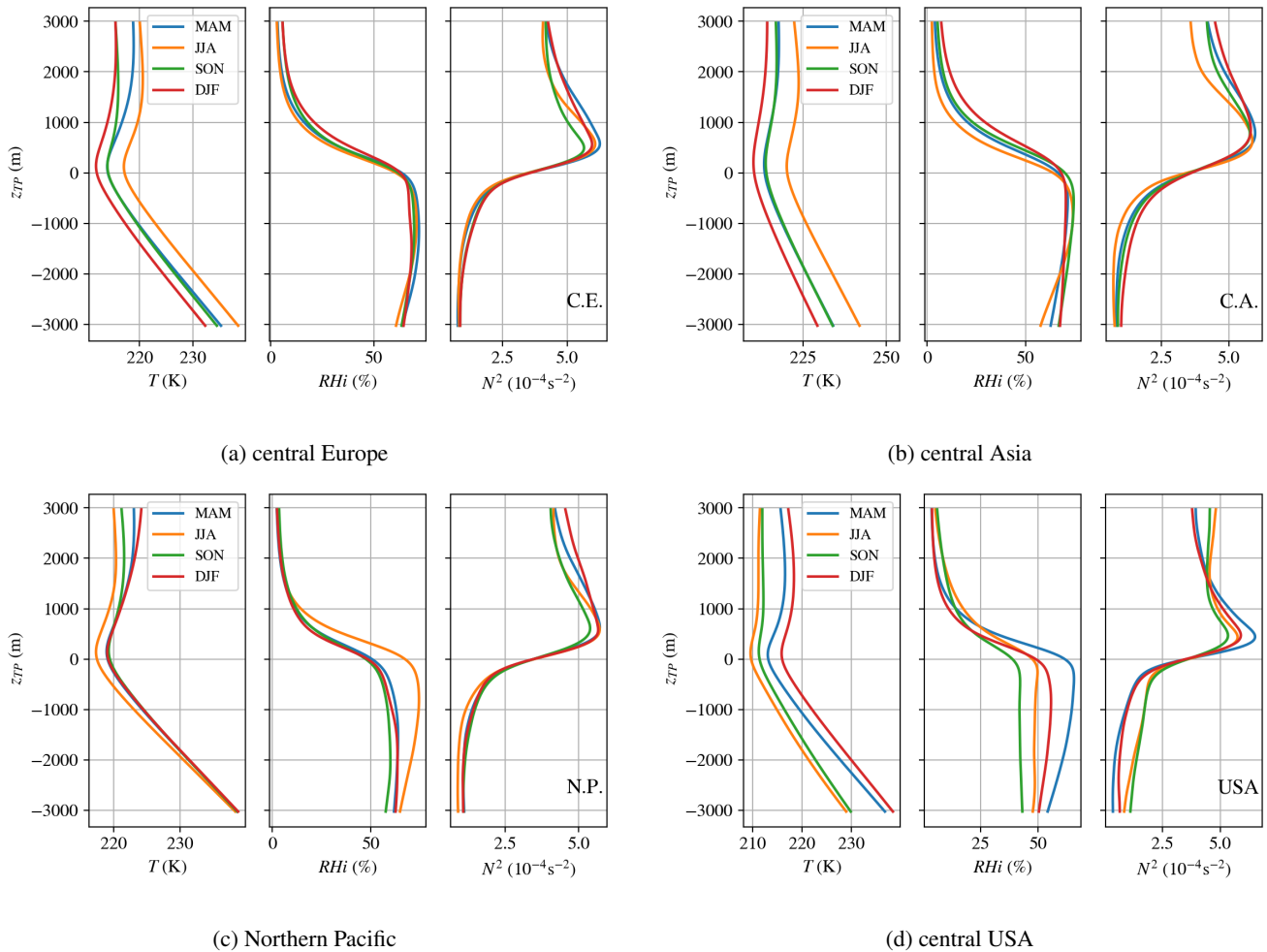
Figure 11. Mean vertical profiles of temperature T, relative humidity over ice RHi and static stability N^2 in the tropopause relative height z_{TP}. Colors indicate the different seasons, i.e., spring months (MAM) in blue, summer months (JJA) in orange, autumn months (SON) in green, and winter months (DJF) in red.

The Northern Pacific region shows small or even no differences in the temperature and RHi profiles between spring, autumn and winter (Fig. 11c). However, the summer season is clearly different, the temperature profile is significantly colder in the tropopause region. At the same time, there is a strong increase in RHi above the first km above the tropopause. This is supporting the idea that water vapour in the UTLS region has a cooling effect on the tropopause region (Randel et al., 2007; 490 Randel and Wu, 2010). The static stability profile shows little seasonal differences, only the autumn months have a smaller static stability peak.

The central USA region shows the strongest seasonal differences in RHi and N^2. The RHi at the tropopause level takes on the highest values in spring followed by winter, summer and autumn in decreasing order. The peaks of N^2 show the similar

pattern with spring exhibiting the strongest peak followed by winter, summer and autumn, respectively. The temperature profile is also different compared to the other regions, with summer exhibiting the lowest and winter the highest temperatures relative to the tropopause. By design the central USA location was introduced to include a region of frequent deep convection in the extratropics. There, significantly higher CAPE values are present in the summer months compared to the other regions (Taszarek et al., 2021), indicating greater deep convection activity. This leads to a stronger seasonal cycle in the vertical profiles in this region.

3.4.2 Seasonal cycle of TIL strength

The correlation between TIL strength and relative humidity is split seasonally using the PDF for different moisture classes for all four regions. The same moisture classes using the average relative humidity with respect to ice (wRHi) as in Fig. 8 are used. The correlation of higher TIL strength (sTIL) values with higher averaged values of wRHi is consistent across every season and every geographical location. Furthermore the correlation of higher sTIL variances with higher wRHi is also present in every region. Also, a distinct feature independent of the geographical region or season is that the low wRHi category shows a mode between $5 \times 10^{-4}\,\mathrm{s}^{-1}$ and $6 \times 10^{-4}\,\mathrm{s}^{-1}$ with a very low occurrence probability above $8 \times 10^{-4}\,\mathrm{s}^{-1}$.

The region over Central Europe and Central USA show a similar seasonal behaviour. The highest values of sTIL (i.e. "strongest TIL") are found in the spring months, while the minima are found in autumn. The winter months show higher variance and stronger extremes compared to summer, which show on average similar sTIL values as in winter. The winter/summer similarity further support the idea (according to Kunkel et al., 2016) that adiabatic processes (i.e. baroclinic forcings) and diabatic processes (e.g. radiative or latent heating) can have similar amplifying effects, although the time scales might not necessarily be the same. The evolution of baroclinic instabilities takes place within days, whereas radiative processes might act on time scales up to few days (if the water vapor concentration is not changed drastically in between). However, cloud processes might act on much shorter scales (minutes to hours). Thus, a clear attribution remains difficult or even impossible. The main difference between central Europe and USA is the considerably higher variance of sTIL in the USA region. Looking at the cyclonic frequencies, the USA region shows a higher frequency than the central Europe across every season. Higher frequency alone does not explain the high variance as the North Pacific with the highest cyclonic frequency do not show higher variance in sTIL. This needs further research in the causes and the forcing mechanisms of the tropopause inversion layer.

The lowest variance of sTIL are found in central Asia (Fig. 12b) across each season and humidity category. Wirth and Szabo (2007) suggested a strengthening of the TIL by baroclinic waves. The baroclinic waves are rare in central Asia as deduced from the low cyclonic frequency, which could explain weaker sTIL values compared to the other region, where baroclinic waves occur more frequently. Also, in Central Asia the highest sTIL values are found in the summer months, which is more characteristic of the polar TIL as demonstrated by Randel et al. (2007) and Grise et al. (2010). This maximum in sTIL in summer observation supports the radiative mechanism suggested by Randel et al. (2007), since the forcing mechanism by baroclinic waves is reduced to a minimum for this region

The region over the Northern Pacific (Fig. 12c) shows a maximum of sTIL values in the winter and spring months, and a similar minimum in autumn and summer. The maxima are most likely due the baroclinic wave activity, which has its maximum
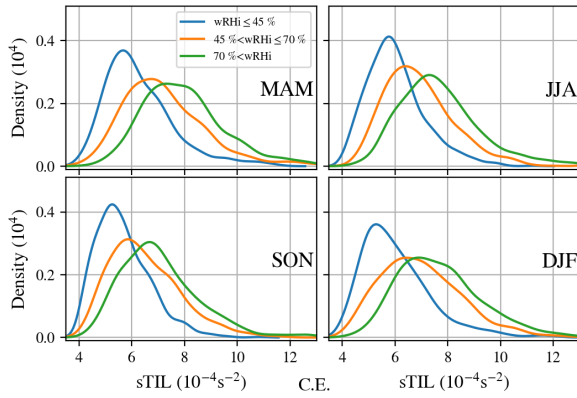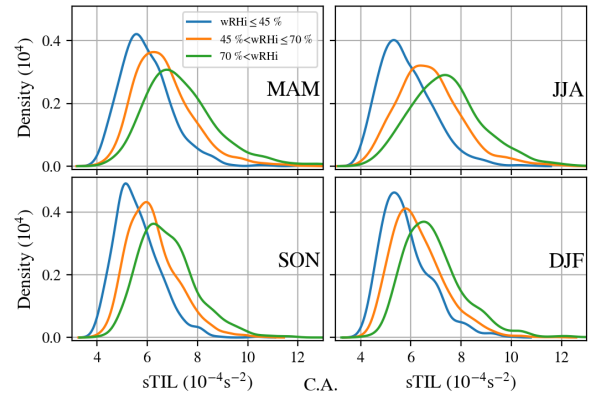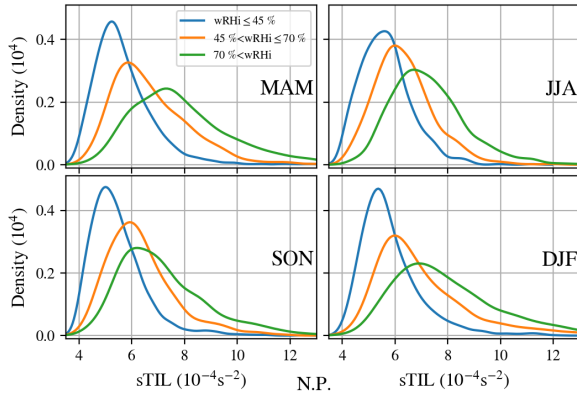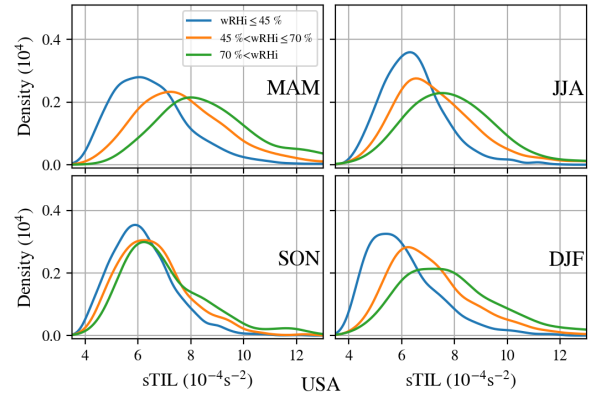
Figure 12. Seasonal probability density distributions of the tropopause inversion layer strength sTIL for categories of average relative humidity over ice wRHi. Colors indicate the different categories. blue: low category (wRHi ≤ 45 %), orange: tmedium category (45 % < wRHi ≤ 70 %), green: high category (70 % < wRHi). The panels represent the behaviour for different resions, i.e., results for Central Europe are shown in (a), for Central Asia in (b), Northern Pacific in (c) and Central USA in (d). In addition, in each subfigure the season is indicated, i.e., spring months (MAM), summer months (JJA), autumn months (SON), and winter months (DJF).

in spring and winter. It is noticeable that the mode in the wettest wRHi category is at higher sTIL values in spring than in winter. This is suggesting that water vapour and its radiative forcing is amplifying the sTIL in spring. The comparison between
530   autumn and summer also shows an interesting aspect. The cyclonic activity has a significant minimum in summer and is lower in autumn than in spring and winter, nonetheless spring and summer are exhibiting similar sTIL values. This gives the indication that the forcing mechanism through baroclinic waves and through the radiative effects might have a similar amplitude, but may act on different time scales.

Altogether, consideration of seasonal and geographic differences reveals the overall robust relationship between the strength of TIL and average humidity with respect to ice in the upper troposphere (wRHi). However, if one looks more closely at the seasonal cycle in different regions with different synoptic characteristics, one finds different processes seen over the year. At the same time evidence for different formation mechanisms for TIL (radiative forcing, baroclinic waves) can be found.

4 Conclusions

From theory and former model investigations we can assume that the variable relative humidity over ice is a very meaningful quantity for the investigations of properties of the tropopause inversion layer. Since the formation and sharpening is first driven by adiabatic compression of the isentropes and afterwards enhanced by irreversible diabatic processes, high values of relative humidity over ice are important marker for both occurring processes. For a detailed investigation we used high resolution radiosonde data over one German site (Idar-Oberstein, 49.69° N, 7.33° E) and the ERA5 data from the reanalysis project of the ECMWF (ERA5 grid point at 49.75° N, 7.25° E). In a first step, we could show that both data agree very well and are both able to represent the TIL and its features quantitatively and qualitatively. In a second step, the properties of the TIL in comparison with some mean relative humidity measure are investigated. As a major result, we find that sharper or stronger TILs occur for higher RHi values, which points to the adiabatic contribution (i.e. adiabatic lifting of the moist layers), and also for sharper gradients of RHi at the moist layer's top, which points to the diabatic processes (e.g. radiative effects). These result are very robust through seasonal variations, as obtained from further analysis of the ERA5 data. In addition, the connection between high humidity values and strong TILs can be found at other extratropical geographical regions, namely Central USA, Central Asia and Northern Pacific at approximately the same latitude througout all seasons. Again, variations in the strength and moisture values might be related to differently strong activity in large scale flows, i.e. in baroclinic instabilities and frontal systems.

Overall, we can state that the ERA5 data is well suited for this kind of investigations, the qualitative features of TILs are well represented. The connection between relative humidity and TIL features is robust and corroborates the former findings in model studies by Kunkel et al. (2016). Although it is not possible to discriminate the adiabatic and diabatic components in the analysis, we could show that the relative humidity is well suited for this kind of analysis, pointing to the relevant processes for the evolution of the tropopause inversion layer.

Code availability. Code for the data processing and analysis is provided on Zenodo (https://zenodo.org/records/10604349).

Data availability. The radiosonde data are publicly available from https://opendata.dwd.de/ at DWD. The ERA5 reanalysis data are publicly available from https://cds.climate.copernicus.eu at ECMWF

Author contributions. DK, PR and PS designed the study; DK carried out the data analyses; DK, PR, and PS contributed to interpreting the results and writing the paper.

Competing interests. The contact author has declared that none of the authors has any competing interests.

565 *Disclaimer.* Publisher's note: Copernicus Publications remains neutral with regard to jurisdictional claims in published maps and institutional affiliations.

Acknowledgements. We thank Deutscher Wetterdienst (DWD) for providing the high resolution radiosonde data, and the European Centre for Medium-Range Weather Forecasts (ECMWF) for providing the ERA5 reanalysis data. We thank Daniel Kunkel for fruitful discussions, and for getting the data from ECMWF. We also thank Peter Hoor for fruitful discussions. Philipp Reutter acknowledges support by the 570 DFG within the Transregional Collaborative Research Centre TRR301 TPChange, Project-ID 428312742 , project C1. Peter Spichtinger acknowledges support by the DFG within the Transregional Collaborative Research Centre TRR301 TPChange, Project-ID 428312742, project B7. The study contributes to the project "Big Data in Atmospheric Physics (BINARY)", funded by the Carl Zeiss Foundation (grant P2018-02-003). The authors thank the two anonymous reviewers for their constructive comments and suggestions that improved the paper.

References

Baumgartner, M., Weigel, R., Harvey, A. H., Plöger, F., Achatz, U., and Spichtinger, P.: Reappraising the appropriate calculation of a common meteorological quantity: potential temperature, Atmospheric Chemistry and Physics, 20, 15 585–15 616, https://doi.org/10.5194/acp-20-15585-2020, 2020.

Bethan, S., Vaughan, G., and Reid, S.: A comparison of ozone and thermal tropopause heights and the impact of tropopause definition on quantifying the ozone content of the troposphere, QUARTERLY JOURNAL OF THE ROYAL METEOROLOGICAL SOCIETY, 122, 929–944, https://doi.org/10.1002/qj.49712253207, 1996.

Birner, T.: Fine-scale structure of the extratropical tropopause region, Journal of geophysical research, 111, https://doi.org/https://doi.org/10.1029/2005JD006301, 2006.

Birner, T.: Residual Circulation and Tropopause Structure, JOURNAL OF THE ATMOSPHERIC SCIENCES, 67, 2582–2600, https://doi.org/10.1175/2010JAS3287.1, 2010.

Birner, T., Dörnbrack, A., and Schumann, U.: How sharp is the tropopause at midlatitudes?, Geophysical Research Letters, 29, https://doi.org/https://doi.org/10.1029/2002GL015142, 2002.

Durran, D. R. and Klemp, J. B.: On the Effects of Moisture on the Brunt-Väisälä Frequency, Journal of the atmospheric sciences, 39, https://doi.org/https://doi.org/10.1175/1520-0469(1982)039<2152:OTEOMO>2.0.CO;2, 1982.

ECMWF: https://confluence.ecmwf.int/display/CKB/ERA5%3A+data+documentation, 2020.

Erler, A. R. and Wirth, V.: The Static Stability of the Tropopause Region in Adiabatic Baroclinic Life Cycle Experiments, Journal of the atmospheric sciences, 68, https://doi.org/https://doi.org/10.1175/2010JAS3694.1, 2011.

Fusina, F. and Spichtinger, P.: Cirrus clouds triggered by radiation, a multiscale phenomenon, Atmospheric Chemistry and Physics, 10, 5179–5190, https://doi.org/10.5194/acp-10-5179-2010, 2010.

Gettelman, A. and Wang, T.: Structural diagnostics of the tropopause inversion layer and its evolution, Journal of geophysical research, 120, https://doi.org/https://doi.org/10.1002/2014JD021846, 2015.

Gettelman, A., Hoor, P., Pan, L. L., Randel, W. J., Hegglin, M. I., and Birner, T.: The Extratropical Upper Troposphere and Lower Stratosphere, Reviews of Geophysics, 49, https://doi.org/https://doi.org/10.1029/2011RG000355, 2011.

Gierens, K., Schumann, U., Helten, M., Smit, H., and Marenco, A.: A distribution law for relative humidity in the upper troposphere and lower stratosphere derived from three years of MOZAIC measurements, ANNALES GEOPHYSICAE-ATMOSPHERES HYDROSPHERES AND SPACE SCIENCES, 17, 1218–1226, https://doi.org/10.1007/s00585-999-1218-7, 1999.

Grise, K. M., J., T. D. W., and Birner, T.: A Global Survey of Static Stability in the Stratosphere and Upper Troposphere, Journal of Climate, https://doi.org/https://doi.org/10.1175/2009JCLI3369.1, 2010.

Hantel, M.: Einführung Theoretische Meteorologie, vol. 1, Springer Spektrum, Springer-Verlag Berlin Heidelberg, 1 edn., https://doi.org/10.1007/978-3-8274-3056-4, 2013.

Hegglin, M. I., Boone, C., Manney, G. L., and Walker, K. A.: A global view of the extratropical tropopause transition layer from Atmospheric Chemistry Experiment Fourier Transform Spectrometer O3, H2O, and CO, Journal of Geophysical Research Atmospheres, 114, https://doi.org/https://doi.org/10.1029/2008JD009984, 2009.

Hersbach, H., Bell, B., Berrisford, P., Hirahara, S., Horányi, A., Muñoz-Sabater, J., Nicolas, J., Peubey, C., Radu, R., Schepers, D., Simmons, A., Soci, C., Abdalla, S., Abellan, X., Balsamo, G., Bechtold, P., Biavati, G., Bidlot, J., Bonavita, M., Chiara, G., Dahlgren, P., Dee, D., Diamantakis, M., Dragani, R., Flemming, J., Forbes, R., Fuentes, M., Geer, A., Haimberger, L., Healy, S., Hogan, R. J., Hólm, E.,

Janisková, M., Keeley, S., Laloyaux, P., Lopez, P., Lupu, C., Radnoti, G., Rosnay, P., Rozum, I., Vamborg, F., Villaume, S., and Thépaut, J.: The ERA5 global reanalysis, Quarterly Journal of the Royal Meteorological Society, 146, 1999–2049, https://doi.org/10.1002/qj.3803, 2020.

Highwood, E. J. and Hoskins, B. J.: The tropical tropopause, Quarterly Journal of the Royal Meteorological Society, 124, 1579–1604, https://doi.org/https://doi.org/10.1002/qj.49712454911, 1998.

Hoerling, M. P., Schaack, T. K., and Lenzen, A. J.: Global Objective Tropopause Analysis, Monthly Weather Review, 119, 1816 – 1831, https://doi.org/10.1175/1520-0493(1991)119<1816:GOTA>2.0.CO;2, 1991.

Hoffmann, L. and Spang, R.: An assessment of tropopause characteristics of the ERA5 and ERA-Interim meteorological reanalyses, Atmospheric Chemistry and Physics, 22, 4019–4046, https://doi.org/10.5194/acp-22-4019-2022, 2022.

Hoinka, K.: The tropopause: discovery, definition and demarcation, METEOROLOGISCHE ZEITSCHRIFT, 6, 281–303, https://doi.org/10.1127/metz/6/1997/281, 1997.

Hoinka, K.: Statistics of the global tropopause pressure, MONTHLY WEATHER REVIEW, 126, 3303–3325, https://doi.org/10.1175/1520-0493(1998)126<3303:SOTGTP>2.0.CO;2, 1998.

Hoskins, B. J. and James, I. N.: Fluid Dynamics of the Midlatitude Atmosphere, Wiley, 1 edn., https://doi.org/10.1002/9781118526002, 2014.

Kunkel, D., Hoor, P., and Wirth, V.: The tropopause inversion layer in baroclinic life-cycle experiments: the role of diabatic processes, Atmospheric Chemistry and Physics, 16, 541–560, https://doi.org/10.5194/acp-16-541-2016, 2016.

Kunz, A., Konopka, P., Müller, R., Pan, L. L., Schiller, C., and Rohrer, F.: High static stability in the mixing layer above the extratropical tropopause, Journal of Geophysical Research Atmospheres, 114, https://doi.org/https://doi.org/10.1029/2009JD011840, 2009.

Kunz, A., Konopka, P., Mueller, R., and Pan, L. L.: Dynamical tropopause based on isentropic potential vorticity gradients, JOURNAL OF GEOPHYSICAL RESEARCH-ATMOSPHERES, 116, https://doi.org/10.1029/2010JD014343, 2011.

Maddox, E. M. and Mullendore, G. L.: Determination of Best Tropopause Definition for Convective Transport Studies, Journal of the Atmospheric Sciences, 75, 3433 – 3446, https://doi.org/10.1175/JAS-D-18-0032.1, 2018.

Miloshevich, L. M., Paukkunen, A., Vömel, H., and Oltmans, S. J.: Development and Validation of a Time-Lag Correction for Vaisala Radiosonde Humidity Measurements, Journal of Atmospheric and Oceanic Technology, 21, https://doi.org/10.1175/1520-0426(2004)021, 2004.

Miloshevich, L. M., Vömel, H., Whiteman, D. N., and Leblanc, T.: Accuracy assessment and correction of Vaisala RS92 radiosonde water vapor measurements, Journal of Geophysical Research Atmospheres, 114, https://doi.org/10.1029/2008JD011565, 2009.

Mullendore, G., Durran, D., and Holton, J.: Cross-tropopause tracer transport in midlatitude convection, JOURNAL OF GEOPHYSICAL RESEARCH-ATMOSPHERES, 110, https://doi.org/10.1029/2004JD005059, 2005.

Murphy, D. M. and Koop, T.: Review of the vapour pressures of ice and supercooled water for atmospheric applications, Quarterly Journal of the Royal Meteorological Society, 131, 1539–1565, https://doi.org/10.1256/qj.04.94, 2005.

Niebler, S., Miltenberger, A., Schmidt, B., and Spichtinger, P.: Automated detection and classification of synoptic-scale fronts from atmospheric data grids, Weather and Climate Dynamics, 3, 113–137, https://doi.org/10.5194/wcd-3-113-2022, 2022.

Pan, L., Randel, W., Gary, B., Mahoney, M., and Hintsa, E.: Definitions and sharpness of the extratropical tropopause: A trace gas perspective, JOURNAL OF GEOPHYSICAL RESEARCH-ATMOSPHERES, 109, https://doi.org/10.1029/2004JD004982, 2004.

Peters, J. M., Mulholland, J. P., and Chavas, D. R.: Generalized Lapse Rate Formulas for Use in Entraining CAPE Calculations, JOURNAL OF THE ATMOSPHERIC SCIENCES, 79, 815–836, https://doi.org/10.1175/JAS-D-21-0118.1, 2022.

Randel, W. J. and Wu, F.: The Polar Summer Tropopause Inversion Layer, Journal of the Atmospheric Sciences, 67, https://doi.org/https://doi.org/10.1175/2010JAS3430.1, 2010.

Randel, W. J., Wu, F., and Forster, P.: The Extratropical Tropopause Inversion Layer: Global Observations with GPS Data, and a Radiative Forcing Mechanism, Journal of Atmospheric Sciences, 64, https://doi.org/https://doi.org/10.1175/2007JAS2412.1, 2007.

Reichler, T., Dameris, M., and Sausen, R.: Determining the tropopause height from gridded data, GEOPHYSICAL RESEARCH LETTERS, 30, https://doi.org/10.1029/2003GL018240, 2003.

Reutter, P., Neis, P., Rohs, S., and Sauvage, B.: Ice supersaturated regions: properties and validation of ERA-Interim reanalysis with IAGOS in situ water vapour measurements, Atmospheric Chemistry and Physics, 20, 787–804, https://doi.org/10.5194/acp-20-787-2020, 2020.

Schmidt, T., Cammas, J.-P., Smit, H. G. J., Heise, S., Wickert, J., and Haser, A.: Observational characteristics of the tropopause inversion layer derived from CHAMP/GRACE radio occultations and MOZAIC aircraft data, Journal of Geophysical Research Atmospheres, 115, https://doi.org/https://doi.org/10.1029/2010JD014284, 2010.

Sonntag, D.: Important new values of the physical constants of 1986, vapour pressure formulations based on the ITS-90, and psychrometer formulae, Zeitschrift für Meteorologie, 40, 1990.

Taszarek, M., Allen, J. T., Marchio, M., and Brooks, H. E.: Global climatology and trends in convective environments from ERA5 and rawinsonde data, npj Climate and Atmospheric Science, 4, https://doi.org/10.1038/s41612-021-00190-x, 2021.

Tinney, E. N., Homeyer, C. R., Elizalde, L., Hurst, D. F., Thompson, A. M., Stauffer, R. M., Vömel, H., and Selkirk, H. B.: A Modern Approach to a Stability-Based Definition of the Tropopause, Monthly Weather Review, 150, 3151 – 3174, https://doi.org/10.1175/MWR-D-22-0174.1, 2022.

Vaisala: https://www.bodc.ac.uk/data/documents/nodb/pdf/RS92SGP-Datasheet-B210358EN-F-LOW.pdf, 2013.

Vaisala: https://www.vaisala.com/sites/default/files/documents/RS-Comparison-White-Paper-B211317EN.pdf, 2014.

Wernli, H. and Schwierz, C.: Surface Cyclones in the ERA-40 Dataset (1958–2001). Part I: Novel Identification Method and Global Climatology, Journal of the Atmospheric Sciences, 63, https://doi.org/https://doi.org/10.1175/JAS3766.1, 2006.

Wirth, V. and Szabo, T.: Sharpness of the extratropical tropopause in baroclinic life cycle experiments, Geophysical Research Letters, 34, https://doi.org/https://doi.org/10.1029/2006GL028369, 2007.

WMO: Meteorology—A three-dimensional science: Second session of the commission for aerology, WMO Bulletin, pp. 136 – 137, 1957.

Xu, H., Guo, J., Tong, B., Zhang, J., Chen, T., Guo, X., Zhang, J., and Chen, W.: Characterizing the near-global cloud vertical structures over land using high-resolution radiosonde measurements, Atmospheric Chemistry and Physics, 23, 15 011–15 038, https://doi.org/10.5194/acp-23-15011-2023, 2023.